Tropical Intraseasonal Variability in DEMETER Seasonal-to-Interannual Prediction Models

Jia-Lin Lin[1], George N. Kiladis[1], Brian E. Mapes[2], and Klaus M. Weickmann[1]

[1]NOAA ESRL/CIRES Climate Diagnostics Center, Boulder, CO
[2]RSMAS, University of Miami, Miami, FL

Submitted to *QJRMS*
November 2006

Corresponding author address: Dr. Jia-Lin Lin
NOAA ESRL/CIRES Climate Diagnostics Center
325 Broadway, R/PSD1, Boulder, CO 80305-3328
Email: jialin.lin@noaa.gov

Abstract

A new challenge for meteorology is dynamical seasonal-to-interannual climate prediction using coupled general circulation models (CGCMs), and many observational and modeling studies have suggested that tropical intraseasonal variability is important for seasonal-to-interannual prediction. This study evaluates tropical intraseasonal variability, especially the fidelity of Madden-Julian Oscillation (MJO) simulations, in three seasonal-to-interannual prediction models participating in the DEMETER (Development of a European Multimodel Ensemble Prediction System for Seasonal-to-Interannual Prediction) project, including the ECMWF, Meteo France, and UKMO models. Eight years of daily precipitation from each model's hindcast experiments are analyzed and compared with daily satellite retrieved precipitation. Space-time spectral analysis is used to obtain the variance and phase speed of the convectively coupled equatorial waves, including Kelvin, equatorial Rossby, mixed Rossby-gravity, and eastward inertio-gravity and westward inertio-gravity waves. The variance and propagation of the MJO, defined as the eastward wavenumbers 1-6, 30-70 day mode, are examined in detail.

The results show that the DEMETER models display a wide range of skill in simulating the tropical intraseasonal variability. The Meteo France model produces quite realistic variances for most of the wave modes including the MJO, as well as a prominent MJO spectral peak and coherent MJO propagation. The ECMWF model simulates reasonable variance for most of the wave modes, but produces overly weak variance for the MJO, and lacks the MJO spectral peak and eastward propagation. The UKMO model produces overly weak variances for most of the wave modes, and lacks the MJO spectral

peak and eastward propagation. The results suggest that the moisture convergence trigger in the convection scheme may play an important role in simulating the MJO.

1. Introduction

A new challenge for meteorology is dynamical seasonal-to-interannual climate prediction using coupled general circulation models (CGCMs; e.g. Shukla et al. 2000; Palmer et al. 2005). The El Nino/Southern Oscillation (ENSO) phenomenon is the dominant interannual mode of the tropical coupled ocean-atmosphere system, and a key to seasonal-to-interannual predictability of the global climate system (e.g. Philander 1990, Wallace et al. 1998, Trenberth et al. 1998, Latif et al. 1998). It affects a wide range of tropical weather and climate, such as the seasonal rainfall within the Asian and Australian monsoons, and the formation and intensity of tropical cyclones. ENSO is a strong tropical heating source, and so is also associated with strengthening and weakening of the zonal mean Hadley circulation, and drives many extratropical teleconnections, such as the Pacific-North-America (PNA) and Pacific-South-America (PSA) patterns. It thus affects high impact midlatitude weather events such as extratropical cyclones, floods, and droughts. Therefore, forecasting of ENSO is central for seasonal-to-interannual climate prediction.

Unfortunately, ENSO is not well simulated or predicted by CGCMs (e.g. Delecluse et al. 1998; Barnston et al. 1999; Latif et al. 2001; Davey et al. 2002; AchutaRao and Sperber 2002, 2006). There is a large scatter in the CGCM simulated ENSO signals, with most of the models producing amplitudes that are too weak and periods that are too short. This is detrimental to the climate prediction of ENSO teleconnections and the potential for high impact weather events, and reflects our limited understanding of ENSO physics.

A promising theory of ENSO is the stochastic forcing theory, which considers ENSO as a stable mode whose growth is influenced by stochastic forcing, or an unstable mode

triggered and/or enhanced by stochastic forcing (e.g., McWilliams and Gent, 1978; Lau, 1985; Penland and Sardeshmukh, 1995; Blanke et al., 1997; Kleeman and Moore, 1997; Eckert and Latif, 1997; Thompson and Battisti, 2001; Dijkstra and Burgers, 2002; Larkin and Harrison, 2002; Kessler, 2002; Zavala-Garay et al., 2003; Perez et al. 2005; Eisenman et al. 2005). Sources of stochastic forcing are considered to be tropical intraseasonal modes such as the Madden-Julian Oscillation (MJO; e.g. Lau and Chan 1986; Weickmann 1991; Kiladis and Weickmann 1992), convectively coupled equatorial waves (e.g. Kiladis et al. 1994; Wheeler and Kiladis 1999; hereafter WK) and tropical cyclones (Keen 1982; Sobel and Camargo 2005), which generate strong westerly wind burst events on the equator. Observational studies have shown that these westerly wind bursts force intraseasonal oceanic Kelvin waves that initiate ENSO events (e.g. Kessler et al. 1995; McPhaden 1999, 2004; Bergman et al. 2001; Roundy and Kiladis 2006), a terminator (e.g. Takayabu et al. 1999; Straub et al. 2006), or a nonlinearly rectified forcing (Kessler and Kleeman 2000). Hindcast experiments of the 1997-98 El Nino event using the ECMWF model (Vitart et al. 2003) demonstrate that reproducing the westerly wind burst events associated with tropical intraseasonal variability is crucial for successfully forecasting an El Nino event, which is corroborated by adjoint model analysis (Van Oldenborgh 2000). Therefore, good simulations of the spectrum of tropical intraseasonal variability is important for CGCMs used for seasonal-to-interannual predictions.

Recently, Palmer et al. (2005) developed a multi-model ensemble-based system for seasonal-to-interannual prediction in a joint European project known as DEMETER (Development of a European Multimodel Ensemble Prediction System for Seasonal to

Interannual Prediction). Comprehensive hindcast evaluation demonstrates the enhanced reliability and skill of the multimodel ensemble over the more conventional single-model ensemble approach. The DEMETER system is being used for making real-time multimodel ensemble seasonal predictions at ECMWF, and the products also lead to better community services such as malaria and crop yield prediction. Apart from the seasonal forecasts, some of the DEMETER models, such as the ECMWF and UKMO models, are also used for real-time global numerical weather prediction. In light of the importance of tropical intraseasonal variability for climate prediction and weather prediction, it seems useful to assess the tropical intraseasonal variability in the DEMETER models. Such an evaluation may help in understanding each model's seasonal and weather forecast skill, and also aid in the improvement of model physics and forecasts.

Many previous studies have evaluated the MJO simulations of GCMs (e.g. Hayashi and Sumi 1986, Hayashi and Golder 1986, 1988, Lau et al. 1988, Slingo et al. 1996; Waliser et al. 2003; Lin et al. 2006). Typically, model MJOs are too weak and propagate too fast. The Atmospheric Model Intercomparison Project (AMIP) study by Slingo et al. (1996) found that no one model captured the dominance of the MJO in space-time spectral analysis found in observations, and nearly all have relatively more power at higher frequencies (<30 days) than in observations.

Recently, Lin et al. (2006) evaluated the tropical intraseasonal variability in 14 CGCMs participating in the Inter-governmental Panel on Climate Change (IPCC) Fourth Assessment Report (AR4). They evaluated not only the MJO, but also, for the first time in the literature, other convectively coupled equatorial waves including the Kelvin,

equatorial Rossby (ER), mixed Rossby-gravity (MRG), eastward inertio-gravity (EIG) and westward inertio-gravity (WIG) waves. The results show that current state-of-the-art GCMs still have significant problems and display a wide range of skill in simulating tropical intraseasonal variability. Apart from representing the disturbances, the total intraseasonal (2-128 day) variance of precipitation is too weak in most of the models. About half of the models have signals of convectively coupled equatorial waves, with Kelvin and MRG-EIG waves especially prominent. However, the variances are generally too weak for all wave modes except the EIG wave, and the phase speeds are generally too fast, suggesting that these models may not have a large enough reduction in their "effective static stability" by diabatic heating. The MJO variance approaches the observed value in only two of the 14 models, but is less than half of the observed value in the other 12 models. The ratio between the eastward versus westward variance is too small in most of the models, which is consistent with the lack of highly coherent eastward propagation of the MJO. Moreover, the MJO variance in 13 of the 14 models does not come from a pronounced spectral peak, but usually comes from part of an over-reddened spectrum, which in turn is associated with too strong persistence of equatorial precipitation.

The purpose of this study is to apply the method of Lin et al. (2006) to evaluate the tropical intraseasonal variability in three DEMETER CGCMs (ECMWF, Meteo France, and UKMO), with an emphasis on their MJO simulations. Two of the three models (ECMWF and UKMO) did not participate in the IPCC AR4 intercomparison by Lin et al. (2006), and therefore it is of use to evaluate their tropical intraseasonal variability. The questions we address are:

(1) How well do the DEMETER models simulate the convectively coupled equatorial waves, especially the MJO?

(2) Do the DEMETER models have similar systematic biases as the IPCC AR4 models?

(3) Is there any systematic dependence of simulated convectively coupled equatorial waves on the basic characteristics of convection scheme, such as closure assumptions? For example, the ECMWF model uses different versions of the same convection scheme (Tiedtke 1989) as the MPI model analyzed by Lin et al. (2006), with the main difference lying in convective trigger. How does this affect the simulation of convectively coupled equatorial waves?

The models and validation datasets used in this study are described in section 2. The diagnostic methods are described in section 3. Results are presented in section 4. A summary and discussion are given in section 5.

2. Models and validation datasets

This analysis is based on eight years of the hindcast experiments from three DEMETER CGCMs. Table 1 shows the model names and acronyms, the resolutions of the atmosphere and ocean GCMs and brief descriptions of their deep convection schemes. Each model conducts 180 days of free coupled runs from an ensemble of initial conditions, starting from four specific days of each year (February 1, May 1, August 1, and November 1). We use the last 128 days of the 180-day hindcast, which is mainly affected by the model rather than the initial condition, since the effect of the initial condition will be significantly reduced after 52 days. For each model we use 6 years of

daily mean surface precipitation from one member of the ensemble runs, which are equivalent in length to about 8 years of a continuous time series.

The model simulations are validated using multiple observational datasets. As in Lin et al. (2006), to bracket the uncertainties associated with precipitation measurements and retrievals, especially the well-known difference between infrared (IR) based retrievals and microwave-based retrievals (e.g. Yuter and Houze 2000), we use two different precipitation datasets: (1) 8 years (1997-2004) of the daily GOES Precipitation Index (GPI, Janowiak and Arkin 1991) precipitation with a horizontal resolution of 2.5 degree longitude by 2.5 latitude, which is retrieved based on IR measurements from multiple geostationary satellites; and (2) 8 years (1997-2004) of daily Global Precipitation Climatology Project (GPCP) One-Degree-Daily (1DD) Precipitation (Huffman et al. 2001) with a horizontal resolution of 1 degree longitude by 1 degree latitude. These are IR-based GPI retrievals scaled by the monthly means of microwave-based SSM/I retrievals.

3. Method

Through the space-time spectral analysis of outgoing longwave radiation (OLR), Takayabu (1994) and WK demonstrated that a significant portion of tropical cloudiness is organized in waves corresponding to the normal modes of the linear shallow water system isolated by Matsuno (1966). In WK, these spectra represent the power remaining in the symmetric and antisymmetric components of OLR about the equator after dividing raw wavenumber-frequency power spectra by an estimate of the background power spectrum. Peaks standing above the background correspond to the Kelvin, n=1 ER,

MRG, n=0 EIG, n=1 WIG and n=2 WIG waves. It was found that the dispersion curves that best match the wavenumber-frequency characteristics of these waves have surprisingly shallow equivalent depths in the range of around 25 m, which is about an order of magnitude smaller than that expected for a free wave with a similar vertical wavelength twice the depth of the troposphere (e.g. Salby and Garcia 1987; Wheeler et al. 2000).

Using the methodology of WK, space-time spectra of daily tropical precipitation were obtained for the 8 years of model data used in this study and compared with those of eight years of observed precipitation estimates from the GPI and 1DD data sets. We will briefly outline this procedure here, and refer the reader to WK and Lin et al. (2006) for further details.

The model and validation precipitation data were first interpolated to a zonal resolution of 5 degrees longitude with the latitudinal resolution varying from model to model (Table 1). We first decomposed the precipitation into its antisymmetric and symmetric components, averaged these from 15N to 15S, and computed spectra of the averaged values. To reduce noise the space-time spectra were calculated as in WK for successive overlapping segments of data and then averaged, here 128 days long with 78 days of overlap between each segment. Complex Fourier coefficients are first obtained in zonal planetary wavenumber space, which are then subjected to a further complex FFT to obtain the wavenumber-frequency spectrum for the symmetric and antisymmetric components of precipitation about the equator.

An estimate of the "background" space-time spectrum is obtained for each data set by averaging the power of the symmetric and antisymmetric spectra and smoothing this by

successive passes of a 1-2-1 filter in frequency and wavenumber (see WK). The raw spectra are then divided by this background to obtain an estimate of the signal standing above the background noise. Here we assume the signal is significant if it stands at 1.2 times (or 20% above) the background. It should be emphasized that, while this is only a rough estimate of the true "significance" of the signals, the intent is to simply identify those modes which might represent signals in rainfall standing above a purely red noise continuum that would presumably prevail if rainfall were not organized by disturbances on the large scale.

The definitions of Kelvin, ER, MRG, EIG and WIG modes are as in WK and Lin et al. (2006). Each mode was isolated by filtering in the wavenumber-frequency domain (see Fig. 6 of WK for the defined regions of filtering for each wave), and the corresponding time series were obtained by an inverse space-time Fourier transform.

As in Lin et al. (2006) the MJO is defined as significant rainfall variability in eastward wavenumber 1-6 and in the period range of 30-70 days. The variance of the MJO anomaly was also compared with the variance of its westward counterpart, i.e., the westward wavenumbers 1 through 6, 30-70 day anomaly, which was isolated using the same method as above.

4. Results

a Climatological precipitation in the equatorial belt

Previous observational studies indicate that the intraseasonal variance of convection is highly correlated with time-mean convective intensity (e.g. Hendon et al. 1999; WK). Therefore we first look at the eight-year time-mean precipitation along the equatorial

belt, especially over the Indo-Pacific warm pool region, where most of the convectively coupled equatorial waves have the largest variance (WK). Figure 1a shows the annual mean precipitation versus longitude averaged between 15N and 15S. To focus on the large-scale features, we smoothed the data zonally to retain only zonal wavenumbers 0-6. All models reproduce the basic feature of observed precipitation, with the primary maximum over the Indo-Pacific warm pool region, and two secondary maxima over Central/South America and Africa. The magnitude of precipitation over the warm pool in all models is close to observations. Within the warm pool region, ECMWF model does not reproduce the local minimum of precipitation over the maritime continent, and there is a tendency for the models to produce more precipitation over the western Pacific than over the eastern Indian Ocean, which is a feature in 1DD data but not in GPI data. Outside the warm pool region, two notable common biases are excessive rainfall over the eastern Pacific and excessive rainfall over Atlantic Ocean.

When the precipitation is averaged over a narrower belt closer to the equator between 5N and 5S, models show a larger scatter in their performance, especially over the western Pacific (Figure 1b). ECMWF produces much greater precipitation than in observations over the western Pacific, and more precipitation over the western Pacific than over the eastern Indian Ocean, a feature that is not observed. Outside the warm pool region, most models reproduce the precipitation minimum over the eastern Pacific trade wind cumulus region reasonably well, but there is a common positive bias over Atlantic Ocean.

In short, the climatological precipitation over the Indo-Pacific warm pool is reasonably simulated by DEMETER models, except that right on the equator over the western Pacific the ECMWF model produces too much precipitation.

b Total intraseasonal (2-128 day) variance and raw space-time spectra

Figure 2 shows the daily standard deviation of the 2-128 day precipitation anomaly along the equator averaged between (a) 15N-15S, and (b) 5N-5S. Two of the three models (ECMWF and Meteo France) reproduce quite well the total intraseasonal variance over the western Pacific both for 15N-15S average (Figure 2a) and 5N-5S average (Figure 2b), as well as the variance over eastern Indian Ocean for 5N-5S average (Figure 2b). However, they do not reproduce well the variance over eastern Indian Ocean for 15N-15S average (Figure 2b). There is a tendency for these models to have larger variance over the western Pacific than over the Indian Ocean, which is consistent with their tendency to have larger annual mean precipitation over the western Pacific (Figure 1). The UKMO model has much weaker variance overall than observations.

The symmetric space-time spectrum of the observed GPI rainfall is shown in Figure 3a. The spectrum of the observed 1DD rainfall is nearly identical to that of GPI (not shown). The spectrum is very similar to those obtained by WK, even though WK used OLR instead of the blend of precipitation estimates comprising the GPI and 1DD data sets. As in WK, the spectra are very red in time and space, with most power at the largest spatial scales and lowest frequencies. Despite this redness, distinct spectral peaks and gaps are evident even in these raw spectra. One obvious feature is the dominance of eastward over westward power at low wavenumbers and frequencies, a signal corresponding to the MJO. Other peaks also correspond to known equatorial wave modes, and will be discussed further below.

The remainder of Figure 3 displays the corresponding symmetric spectra from the various models examined for this study, using identical contour intervals and shading as

in Figure 3a (recall that these spectra are calculated for identical daily and 5 degree horizontal resolutions). The two models with large total intraseasonal variance (ECMWF and Meteo France; Figure 2) have spectra that are broadly similar to observed spectra, except that ECMWF has much less power than observed at low wavenumbers and frequencies (wavenumbers 1-6, period > 30 days) and lacks the dominance of eastward over westward power, implying standing oscillations rather than the predominance of eastward power in observations. The UKMO model, which has weak total intraseasonal variance (Figure 2), also has much less power than observed at all wavenumbers and frequencies. The characteristics of the antisymmetric spectra, in terms of total power and redness, are generally similar to Figure 3 and so will not be shown here.

In summary, the ECMWF and Meteo France models produce realistic total intraseasonal (2-128 day) variance of precipitation, especially over the western Pacific. Their space-time spectra are similar to the observed spectra, except that ECMWF has much less power than observed at low wavenumbers and frequencies (wavenumbers 1-6, period > 30 days). The UKMO model has much weaker variance than observations, and its space-time spectra have much less power than observed at all wavenumbers and frequencies.

c Dominant intraseasonal modes

Figure 4 and Figure 5 show the results of dividing the symmetric and antisymmetric raw spectra by the estimates of their background spectra. This normalization procedure removes a large portion of the systematic biases within the various models and observed data sets in Figure 3, more clearly displaying the model disturbances with respect to their own climatological variance at each scale. Signals of the Kelvin, ER, and WIG waves are

readily identified in the observational symmetric spectra (Figure 4a), along with the MRG and EIG waves in the antisymmetric spectra (Figure 5a). The MJO also appears as a prominent signal, especially in the symmetric spectra. Dispersion curves of the shallow water modes are also shown on all spectra, corresponding to equivalent depths of 8, 12, 25, 50, and 90 m. As in the OLR spectra of WK, the spectral peaks corresponding to shallow water modes best match an equivalent depth of around 25 m in the observational rainfall data.

All of the models appear to have signals of convectively coupled waves, with the symmetric modes (Kelvin, ER, and WIG) especially prominent. Based on the equivalent depths, the phase speeds of the waves are nearly realistic in the ECMWF and Meteo France models, but are too fast in the UKMO model. Interestingly, this scaling is consistent within a given model across modes, i.e. all modes scale similarly to a certain equivalent depth within a given pair of symmetric and antisymmetric spectra, which is indicative of similar physical processes linking the convection and large scale disturbances within each model and in the real atmosphere.

When a model displays signals of a certain wave mode in Figure 4 and Figure 5, it means that the variance of that wave mode stands out above the background spectra (i.e., exhibiting a high signal-to-noise ratio), but the absolute value of the variance of that wave mode may not be large. Therefore, it is of interest to look further at the absolute values of the variance of each significant wave mode. Figure 6 shows the variances of the symmetric wave modes, including (a) Kelvin, (b) ER, and (c) WIG modes along the equator averaged between 15N and 15S. The two models with realistic total intraseasonal variance (ECMWF and Meteo France) also produce large variances for these wave

modes, suggesting that wave-heating feedback is relatively strong in these models, which is consistent with the nearly realistic phase speeds of waves in these models. On the contrary, the model with too weak total intraseasonal variance (UKMO) also produces weak variances for the Kelvin and WIG waves, suggesting that the models do not have enough wave-heating feedback in those waves, which is consistent with the too-fast phase speeds of those waves in the model. However, UKMO produces large ER variance, which is in sharp contrast with its inability in simulating other modes. This is very interesting and warrants further study. The variances of the antisymmetric wave modes are not shown because they are generally not statistically significant in the models (Figure 5).

In summary, all of the models appear to have signals of convectively coupled waves, with Kelvin, ER, and WIG waves especially prominent. The ECMWF and Meteo France models produce nearly realistic phase speed and large variance for these wave modes, while the UKMO model simulates too-fast phase speed for the wave modes and too-small variance for Kelvin and WIG waves, but large variance for the ER wave.

d Variance of the MJO mode

Now we focus on the variance of the MJO mode, i.e., the daily variance in the MJO window of eastward wavenumbers 1-6 and periods of 30-70 days. Figure 7 shows the variance of the MJO anomaly along the equator averaged between 15N and 15S. The MJO variance approaches the observed value in the Meteo France model, but is less than half of the observed value in ECMWF and UKMO models. Too weak precipitation variance in the MJO wavenumber-frequency band has been a long-standing problem in GCMs, in spite of the fact that many of these models have reasonable values of zonal

wind variance. From the viewpoint of weather and climate prediction, a realistic MJO precipitation signal is more desirable because it is the latent heat released by precipitation that drives teleconnections to the subtropics and extratropics and leads to useful predictability.

In addition to the variance, another important characteristic of the observed MJO is its eastward propagation. A useful method for evaluating the MJO propagation is to look at the propagation of the 30-70 day filtered anomaly of the raw precipitation data, which includes all wavenumbers, to see if the MJO mode (the eastward wavenumbers 1-6 mode) dominates over other modes, as is the case in observations (e.g. Weickmann et al. 1985, 1997, Kiladis and Weickmann 1992, Lin and Mapes 2004). Because the tropical intraseasonal oscillation is dominated by zonally asymmetric, planetary-scale phenomena, the competition is mainly between the MJO and its westward counterpart - the westward wavenumber 1-6 component. Figure 8 shows the lag-correlation of 30-70 day precipitation anomaly averaged between 5N and 5S with respect to itself at 0N85E. Both observational data sets show prominent eastward propagating signals of the MJO, with a phase speed of about 7 m/s. The Meteo France model displays a highly coherent eastward propagating signal, although the phase speed is a little too slow. The ECMWF and UKMO models, however, show primarily standing oscillations. The results are similar when using a western Pacific reference point (not shown).

Next we apply more detailed scrutiny to the MJO precipitation variance by looking at the shape of the power spectrum. Figure 9 shows the spectra of the eastward wavenumber 1-6 component at 0N85E. Both of the two observational datasets show prominent spectral peaks between 30 and 70 days periods, with the power of 1DD lower than that of the

GPI. The Meteo France model shows a pronounced spectral peak in the MJO frequency band. The ECMWF and UKMO models lack a pronounced spectral peak, but show too red of a spectrum, i.e., the variance of the MJO band does not stand above but is simply embedded within a red noise continuum. Results for 0N155E (western Pacific) are similar (not shown).

The redness of spectra shown in Figure 9 is reminiscent of a "red noise" spectrum of a first-order linear Markov process (Gilman 1963; Jenkins and Watts 1968; Lin et al. 2006). For the first-order Markov process, the redness of the spectrum is determined by its lag-one auto-correlation ρ, which is hereafter referred to as the persistence of the time series. Therefore we plot in Figure 10 the auto-correlation function of precipitation at 0N85E. Both observational datasets have a ρ of about 0.7. The ECMWF and Meteo France models have nearly realistic values of ρ, while the UKMO model has a ρ significantly larger than the observed value, consistent with its spectrum being too red (Figure 9). It is interesting to see that ECMWF model has a realistic ρ in spite of its red spectrum, which may be associated with the peak at around 30 days in its spectrum (Figure 9). Results for 0N155E (western Pacific) are similar (not shown).

To summarize, the Meteo France model produces nearly realistic MJO variance, eastward propagation of MJO, and the prominent MJO spectral peak, although the phase speeds of the MJO is a little too slow. The ECMWF and UKMO models produce too weak MJO variance that is less than half of the observed value, and lack the eastward propagation or MJO spectral peak, with the MJO variance coming from part of an over-reddened spectrum. The over-reddened spectrum in the UKMO model is associated with overly strong persistence of equatorial precipitation.

5. Summary and discussion

Many observational and modeling studies have suggested that tropical intraseasonal variability is important for seasonal-to-interannual prediction. This study evaluates tropical intraseasonal variability, especially the fidelity of MJO simulations, in three seasonal-to-interannual prediction models participating in the DEMETER project, including the ECMWF, Meteo France, and UKMO models. Eight years of daily precipitation from each model's hindcast experiments are analyzed and compared with daily satellite retrieved precipitation. Space-time spectral analysis is used to obtain the variance and phase speed of the convectively coupled equatorial waves, including Kelvin, equatorial Rossby, mixed Rossby-gravity, and eastward inertio-gravity and westward inertio-gravity waves. The variance and propagation of the MJO, defined as the eastward wavenumbers 1-6, 30-70 day mode, are examined in detail.

The results show that the DEMETER models display a wide range of skill in simulating the tropical intraseasonal variability. The Meteo France model produces quite realistic variances for most of the wave modes including the MJO, as well as a prominent MJO spectral peak and coherent MJO propagation. The ECMWF model simulates reasonable variance for most of the wave modes, but produces overly weak variance for the MJO, and lacks the MJO spectral peak and eastward propagation. The UKMO model produces overly weak variances for most of the wave modes, and lacks the MJO spectral peak and eastward propagation.

Factors hypothesized to be important for MJO simulations include model physics, model resolution, and air-sea coupling. Regarding the model physics, our results demonstrate three important points. First, the model that arguably does best at simulating

the convectively coupled equatorial waves including the MJO (Meteo France) has its convective closures linked to moisture convergence. For the AMIP models, Slingo et al. (1996) found that deep convection schemes with CAPE-type closure tend to produce more realistic MJO signals than schemes with moisture-convergence-type closure, but we find a reverse dependence in the DEMETER models, as did Lin et al. (2006) for a variety of other models participating IPCC AR4. One possible reason is that the moisture-convergence-type closures/triggers tie the convection more closely with large-scale wave circulation and thus enhance the wave-heating feedback in the MJO.

Second, models producing good signals for other convectively coupled equatorial waves do not necessarily simulate good MJO signals (e.g. ECMWF). Interestingly, the ECMWF model uses a different version of the same deep convection scheme, the Tiedke (1989) scheme, as the MPI model analyzed by Lin et al. (2006), which produces quite realistic MJO signals. The main difference between the two versions of Tiedke scheme lies in the convective trigger with the MPI model using a moisture convergence trigger while the ECMWF model using an instability trigger. The fact that MPI produces good MJO signals but ECMWF does not suggests that the moisture convergence trigger may play an important role in simulating the MJO.

Third, the overly red spectrum of precipitation in the UKMO model is closely tied to its overly strong persistence of equatorial precipitation. As discussed by Lin et al. (2006), the persistence of equatorial precipitation is strongly affected by subgrid scale processes, and may be improved by improving a model's moist physics, for example, by including the self-suppression processes in tropical deep convection such as moisture triggers, convective downdrafts, and mesoscale downdrafts.

As discussed in the introduction, observational and modeling studies have shown that the tropical intraseasonal variability plays an important role in triggering, terminating and possibly maintaining ENSO events. Therefore, the wide range of skill in simulating the tropical intraseasonal variability by the DEMETER models may affect their seasonal-to-interannual prediction skills. In future studies, it would be interesting to compare the evolution of ENSO events in different models to examine how the different behaviors of intraseasonal variability affect the ENSO initiation and amplification.

Acknowledgements

We would like to thank Tim Palmer for the information about the DEMETER project. J. L. Lin was supported by the NASA Modeling, Analysis and Prediction (MAP) Program, NOAA CPO/CVP Program, and NOAA CPO/CDEP Program. GNK was supported by the NOAA CPO under Grant GC01-351.

REFERENCES

AchutaRao, K., and K. R. Sperber, 2002: Simulation of the El Niño Southern Oscillation: results from the coupled model intercomparison project, *Clim. Dyn., 19,* 191–209.

AchutaRao, K., and K. R. Sperber, 2006: ENSO Simulation in Coupled Ocean-Atmosphere Models: Are the Current Models Better? *Climate Dyn.*, 10.1007/s00382-006-0119-7.

Barnston, A. G., Y. He, and M. H. Glantz, 1999: Predictive skill of statistical and dynamical climate models in SST forecasts during the 1997–98 El Niño episode and the 1998 La Niña onset, *Bull. Amer. Meteor. Soc., 80*, 217–244.

Bergman, J. W., H. H. Hendon, K. M.Weickmann, 2001: Intraseasonal Air-Sea Interactions at the Onset of El Nino. *J. Climate*, **14**, 1702-1719.

Blanke, B., J. D. Neelin, and D. Gutzler, 1997: Estimating the effect of stochastic wind stress forcing on ENSO irregularity, *J. Climate, 10*, 1473–1486.

Bougeault, P., 1985: A Simple Parameterization of the Large-Scale Effects of Cumulus Convection. *Monthly Weather Review*, 113, 2108–2121.

Davey, M. K., and coauthors, 2002: STOIC: a study of coupled model climatology and variability in tropical ocean regions, *Clim. Dyn., 18*, 403–420.

Delecluse, P., M. Davey, Y. Kitamura, S. Philander, M. Suarez, and L. Bengtsson, 1998: Coupled general circulation modeling of the tropical Pacific. *J. Geophys. Res.,* **103**, 14357–14373.

Duchan, C.E., 1979: Lanczos filtering in one and two dimensions. *J. Appl. Meteor.*, **18**, 1016-1022.

Dijkstra, H. A., and G. Burgers, 2002: Fluid dynamics of El Niño variability. *Annu. Rev.*

Fluid Mech., **34**, 531–558.

Eckert, C., and M. Latif, 1997: Predictability of a stochastically forced hybrid coupled model of El Niño, *J. Climate, 10*, 1488–1504.

Eisenman, I., Lisan Yu and Eli Tziperman. 2005: Westerly Wind Bursts: ENSO's Tail Rather than the Dog?. *J. Climate*, 18, 5224–5238.

Emanuel, K. A., J. D. Neelin, and C. S. Bretherton, 1994: On large-scale circulations in convecting atmospheres. *Quart. J. Roy. Meteor. Soc.,* **120,** 1111–1143.

Flatau, M., P.J. Flatau, P. Phoebus, and P.P. Niiler, 1997: The feedback between equatorial convection and local radiative and evaporative processes: The implications for intraseasonal oscillations. *J. Atmos. Sci*., **54**, 2373-2386.

Gill, A. E., 1982: Studies of moisture effects in simple atmospheric models: The stable case. *Geophys. Astrophys. Fluid Dyn.,* **19,** 119–152.

Gregory, D., J. J. Morcrette, C. Jakob, A. C. M. Beljaars, and T. Stockdale, 2000: Revision of convection, radiation and cloud schemes in the ECMWF Integrated Forecasting System. *Quart. J. Roy. Meteor. Soc.,* **126,** 1685–1710.

Gutzler, D. S., 1991: Interannual fluctuations of intraseasonal variance of near-equatorial zonal winds. *J. Geophys. Res.,* **96,** 3173–3185.

Hayashi, Y., and A. Sumi, 1986: The 30-40 day oscillation simulated in an"aqua planet" model. *J. Meteor. Soc. Japan.*, **64**, 451-466.

Hayashi, Y., and D. G. Golder, 1986: Tropical intraseasonal oscillations appearing in a GFDL general circulation model and FGGE data. Part I: Phase propagation. *J. Atmos. Sci.*, **43**, 3058-3067.

Hayashi, Y., and D. G. Golder, 1988: Tropical intraseasonal oscillations appearing in a GFDL general circulation model and FGGE data. Part II: Structure. *J. Atmos. Sci.*, **45**, 3017-3033.

Hendon, H.H., C. Zhang, and J.D. Glick, 1999: Interannual variation of the MJO during austral summer. *J. Climate*, **12**, 2538-2550.

Huffman, G.J., R.F. Adler, M.M. Morrissey, S. Curtis, R. Joyce, B. McGavock, and J. Susskind, 2001: Global precipitation at one-degree daily resolution from multi-satellite observations. *J. Hydrometeor.*, **2**, 36-50.

Janowiak, J. E., and P. A. Arkin, 1991: Rainfall variations in the Tropics during 1986-1989, as estimated from observations of cloud-top temperatures. *J. Geophys. Res.*, **96** (Suppl.), 3359-3373.

Keen, R. A., 1982: The role of cross-equatorial cyclone pairs in the Southern Oscillation. *Mon. Wea. Rev.,* **110,** 1405–1416.

Kessler, W. S., 2002: Is ENSO a cycle or a series of events? *Geophys. Res. Lett., 29(23)*, 2125, doi:10.1029/2002GL015924.

Kessler, W. S., and R. Kleeman, 2000: Rectification of the Madden-Julian Oscillation into the ENSO cycle, *J. Climate, 13,* 3560–3575.

Kessler, W. S., and M. J. McPhaden, and K. M. Weickmann, 1995: Forcing of intraseasonal Kelvin waves in the equatorial Pacific. *J. Geophys. Res.*, **100**, 10613-10631.

Kiladis, G.N., G.A. Meehl, and K.M. Weickmann, 1994: Large-scale circulation associated with westerly wind bursts and deep convection over the western equatorial Pacific. *J. Geophys. Res.*, **99**, D9, 18,527-18-544.

Kiladis, G. N., K. H. Straub, and P. T. Haertel, 2005: Zonal and vertical structure of the Madden-Julian Oscillation. *J. Atmos. Sci.*, **62**, 2790-2805.

Kiladis, G. N. and K. M. Weickmann, 1992: Circulation anomalies associated with tropical convection during northern winter. *Mon. Wea. Rev.,* **120**, 1900-1923.

Kleeman, R., and A. M. Moore, 1997: A theory for the limitation of ENSO predictability due to stochastic atmospheric transients, *J. Atmos. Sci., 54*, 753–767.

Latif, M., D. Anderson, T. Barnett, M. Cane, R. Kleeman, A. Leetmaa, J. O'Brien, A. Rosati, and E. Schneider, 1998: A review of the predictability and prediction of ENSO, *J. Geophys*. *Res., 103*, 14375–14393.

Latif, M., and coauthors, 2001: ENSIP: the El Niño simulation intercomparison project, *Clim. Dyn., 18*, 255–276.

Lau. K. M., and P.H. Chan. 1986: The 40–50 Day Oscillation and the El Niño/Southern Oscillation: A New Perspective. *Bull. Amer. Meteor. Soc.*, 67, 533–534.

Lau, N. C., I. M. Held, and J. D. Neelin, 1988: The Madden-Julian oscillations in an idealized general circulation model. *J. Atmos. Sci.*, **45**, 3810-3831.

Lee, M.-I., I.-S. Kang, J.-K. Kim, and B. E. Mapes, 2001: Influence of cloud-radiation interaction on simulating tropical intraseasonal oscillation with an atmospheric general circulation model , *J. Geophys. Res.*, **106**, 14219-14233.

Lee, M.-I., I.-S. Kang, and B.E. Mapes, 2003: Impacts of cumulus convection parameterization on aqua-planet AGCM simulations of tropical intraseasonal variability. *J. Meteor. Soc. Japan,* **81**, 963-992.

Lin, J. L., and B. E. Mapes, 2004: Radiation budget of the tropical intraseasonal oscillation. *J. Atmos. Sci.*, **61**, 2050-2062.

Lin, J. L., B. E. Mapes, M. H. Zhang and M. Newman, 2004: Stratiform precipitation, vertical heating profiles, and the Madden-Julian Oscillation. *J. Atmos. Sci.*, **61**, 296-309.

Lin, J. L., M. H. Zhang, and B. E. Mapes, 2005: Zonal momentum budget of the Madden-Julian Oscillation: The sources and strength of equivalent linear damping. *J. Atmos. Sci*., **62**, 2172-2188.

Lin, J.L., G.N. Kiladis, B.E. Mapes, K.M. Weickmann, K.R. Sperber, W.Y. Lin, M. Wheeler, S.D. Schubert, A. Del Genio, L.J. Donner, S. Emori, J.-F. Gueremy, F. Hourdin, P.J. Rasch, E. Roeckner, and J.F. Scinocca, 2006: Tropical intraseasonal variability in 14 IPCC AR4 climate models. Part I: Convective signals. *J. Climate*, **19**, 2665-2690.

Love, G., 1985: Cross-equatorial influence of winter hemisphere subtropical cold surges. *Mon. Wea. Rev.,* **113,** 1487–1498.

Majda, A. J., and J. A. Biello, 2004: A multi-scale model for tropical intraseasonal oscillations. *Proc. Natl. Acad. Sci.,* **101**, 4736–4741.

Majda, A. J., J. Biello, 2005: A New Multi-Scale Model for the Madden-Julian Oscillation. *J. Atmos. Sci.*, **62**, 1694–1721.

Mapes, B. E., and R. A. Houze, 1995: Diabatic divergence profiles in western Pacific mesoscale convective systems. *J. Atmos. Sci.*, **52**, 1807-1828.

Mapes, B. E., and J. L. Lin, 2005: Doppler radar observations of mesoscale wind divergence in regions of tropical convection. *Mon. Wea. Rev*., in press.

Matsuno, T., 1966: Quasi-geostrophic motions in the equatorial area. *J. Meteor. Soc. Japan,* **44,** 25–43.

McPhaden, M. J., 1999: Genesis and evolution of the 1997–98 El Niño. *Science,* **283,** 950–954.

McPhaden, M.J., 2004: Evolution of the 2002–2003 El Niño. *Bull. Amer. Meteor. Soc., 85*, 677–695.

McWilliams, J., and P. Gent, 1978: A coupled air-sea model for the tropical Pacific, *J. Atmos. Sci., 35*, 962–989.

Moore, A. M., and R. Kleeman, 1996: The dynamics of error growth and predictability in a coupled model of ENSO, *Q. J. R. Meteorol. Soc., 122*, 1405–1446.

Nordeng, T.E., 1994: Extended versions of the convective parameterization scheme at ECMWF and their impact on the mean and transient activity of the model in the tropics. Technical Memorandum No. 206, European Centre for Medium-Range Weather Forecasts, Reading, United Kingdom.

Palmer, T. N., A. Alessandri, U. Andersen, P. Cantelaube, M. Davey, P. Délécluse, M. Déqué,, E. Díez, F. J. Doblas-Reyes, H. Feddersen, R. Graham, S. Gualdi, J.-F. Guérémy, R. Hagedorn, M. Hoshen, N. Keenlyside, M. Latif, A. Lazar, E. Maisonnave, V. Marletto, A. P. Morse, B. Orfila, P. Rogel, J.-M. Terres and M. C. Thomson. 2004: Development of a European Multimodel Ensemble System for Seasonal-to-Interannual Prediction (DEMETER). *Bull. Amer. Meteor. Soc.*, **85**, 853–872.

Penland, C., and P. D. Sardeshmukh, 1995: The optimal growth of tropical sea surface temperature anomalies, *J. Climate, 8*, 1999–2024.

Perez, C. L., Andrew M. Moore, Javier Zavala-Garay and Richard Kleeman. 2005: A Comparison of the Influence of Additive and Multiplicative Stochastic Forcing on a Coupled Model of ENSO. *J. Climate*, 18, 5066–5085.

Philander, S. G., 1990: *El Niño, La Niña, and the Southern Oscillation*, Academic Press, London, 289 pp.

Roundy, P., and G. N. Kiladis, 2006: Observed relationships between oceanic Kelvin waves and atmospheric forcing. *J. Climate*, **19**, 5253-5272.

Schubert, S., R. Dole, H.v.d. Dool, M. Suarez, and D. Waliser, 2002: Proceedings from a workshop on ”Prospects for improved forecasts of weather and short-term climate variability on subseasonal (2 week to 2 month) time scales”, 16-18 April 2002, Mitchellville, MD, NASA/TM 2002-104606, vol. 23, pp. 171.

Shukla, J., J. Anderson, D. Baumhefner, C. Brankovic, Y. Chang, E. Kalnay, L. Marx, T. Palmer, D. Paolino, J. Ploshay, S. Schubert, D. Straus, M. Suarez and J. Tribbia. 2000: Dynamical Seasonal Prediction. *Bulletin of the American Meteorological Society*, 81, 2593–2606.

Slingo, J. M., and Coauthors, 1996: Intraseasonal oscillations in 15 atmospheric general circulation models: Results from an AMIP diagnostic subproject. *Climate Dyn.*, **12**, 325-357.

Sobel, A. H., and S. Camargo, 2005: Influence of western Pacific tropical cyclones on their large-scale environment. J. Atmos. Sci., 62, 3396-3407.

Straub, K. H., G. N. Kiladis, and P. E. Ciesielski, 2006: The role of equatorial waves in the onset of the South China Sea summer monsoon and the demise of El Niño during 1998. Dyn. Atmos. Oceans, doi:10.1016/j.dynatmoce.2006.02.005.

Takayabu, Y .N., T. Iguchi, M. Kachi, A. Shibata, and H. Kanzawa, 1999: Abrupt termination of the 1997-98 El Nino in response to a Madden-Julian oscillation. *Nature*, **402**, 279-282.

Tiedke, M., 1989: A comprehensive mass flux scheme for cumulus parameterization in large-scale models. *Mon. Wea. Rev.,* **117**, 1779-1800.

Thompson, C. J., and D. S. Battisti, 2001: A linear stochastic dynamical model of ENSO. Part II: Analysis, *J. Climate*, 14, 445–466.

Trenberth, K. E., G. W. Branstator, D. Karoly, A. Kumar, N.-C. Lau, and C. Ropelewski, 1998: Progress during TOGA in understanding and modeling global teleconnections associated with tropical sea surface temperatures. *J. Geophys. Res.,* **103,** 14 291–14 324.

van Oldenborgh, G. J., 2000: What Caused the Onset of the 1997–98 El Niño? Mon. Wea. Rev., 128,2601-2607.

Vitart, F., M. A. Balmaseda, L. Ferranti, and D. Anderson, 2003: Westerly Wind Events and the 1997/98 El Niño Event in the ECMWF Seasonal Forecasting System: A Case Study. J. Climate, 16, 3153-3170.

Waliser, D., S. Schubert, A. Kumar, K. Weickmann, and R. Dole, 2003b: Proceedings from a workshop on ”Modeling, Simulation and Forecasting of Subseasonal Variability”, NASA/CP 2003-104606, vol. 25, pp. 62.

Wallace, J. M., E. M. Rasmusson, T. P. Mitchell, V. E. Kousky, E. S. Sarachik, and H. von Storch, 1998: On the structure and evolution of ENSO-related climate variability in the tropical Pacific: Lessons from TOGA. *J. Geophys. Res.,* **103,** 14 241–14 260.

Wang, W., and M.E. Schlesinger, 1999: The dependence on convective parameterization of the tropical intraseasonal oscillation simulated by the UIUC 11-layer atmospheric GCM. *J. Climate*, **12**, 1423-1457.

Weickmann, K. M., 1991: El Nino Southern Oscillation and Madden- Julian (30-60 day) oscillations during 1981-82. J. Geophys. Res., 96, Supplement, 3187-3195.

Weickmann, K. M., G. R. Lussky, and J. E. Kutzbach, 1985: Intraseasonal (30-60 day) fluctuations of outgoing longwave radiation and 250 mb streamfunction during northern winter. *Mon. Wea. Rev.*, **113**, 941-961.

Weickmann, K., G. Kiladis and P. Sardeshmukh, 1997: The dynamics of intraseasonal atmospheric angular momentum oscillations. J. Atmos. Sci., 54, 1445-1461.

Wheeler, M., and G.N. Kiladis, 1999: Convectively Coupled Equatorial Waves: Analysis of Clouds and Temperature in the Wavenumber-Frequency Domain. *J. Atmos. Sci.,* **56**, 374-399.

Wheeler, M., G.N. Kiladis, and P.J. Webster, 2000: Large-scale dynamical fields associated with convectively coupled equatorial waves. *J. Atmos. Sci.*, 57, 613-640.

Xie, P., and P. A. Arkin, 1997: Global precipitation: A 17-year monthly analysis based on gauge observations, satellite estimates, and numerical model outputs. *Bull. Amer. Meteor. Soc.*, **78**, 2539-2558.

Yuter, S. E., and R. A. Houze Jr.. 2000: The 1997 Pan American Climate Studies Tropical Eastern Pacific Process Study. Part I: ITCZ Region. *Bulletin of the American Meteorological Society*, 81, 451–481.

Zavala-Garay, J., A. M. Moore, C. L. Perez, and R. Kleeman, 2003: The response of a coupled mode of ENSO to observed estimates of stochastic forcing, *J. Climate, 16*, 2827–2842.

FIGURE CAPTIONS

Figure 1. Annual mean precipitation along the equatorial belt averaged between (a) 15N and 15S, and (b) 5N and 5S for two observational datasets and 14 models. The data are smoothed zonally to keep only wavenumber 0-6. The locations of continents within the equatorial belt are indicated by black bars under the abscissa.

Figure 2. Variance of the 2-128 day precipitation anomaly along the equator averaged between (a) 15N-15S, and (b) 5N-5S.

Figure 3. Space-time spectrum of 15N-15S symmetric component of precipitation. Frequency spectral width is 1/128 cpd.

Figure 4. Space-time spectrum of 15N-15S symmetric component of precipitation divided by the background spectrum. Superimposed are the dispersion curves of the odd meridional mode-numbered equatorial waves for the five equivalent depths of 8, 12, 25, 50, and 90m. Frequency spectral width is 1/128 cpd.

Figure 5. Same as Figure 4 but for the antisymmetric component.

Figure 6. Variances of (a) Kelvin, (b) ER, and (c) WIG modes along the equator averaged between 15N and 15S.

Figure 7. Variance of the MJO mode along the equator averaged between 15N and 15S.

Figure 8. Lag-correlation of the 30-70 day precipitation anomaly averaged along the equator between 5N and 5S with respect to itself at 0N85E. Shading denotes the regions where lag-correlation is above the 95% confidence level. The three thick lines correspond to phase speed of 3, 7, and 15 m/s, respectively.

Figure 9. Spectrum of the eastward wavenumber 1-6 component of equatorial precipitation (5N-5S) at 0N85E for two observational datasets and 14 models. Upper

panel: raw spectrum; Lower panel: normalized spectrum. Frequency spectral width 1/100 cpd.

Figure 10. Auto-correlation of precipitation at 0N85E.

Table 1 List of models that participate in this study

Models	AGCM Grid type/ Resolution	AGCM Deep convection scheme	AGCM Closure/ Trigger	OGCM resolution	OGCM flux correction
ECMWF	Spectral T95*L40	Tiedke (1989)/ Nordeng (1994) Gregory et al. (2000)	CAPE/ CAPE	1.4*0.3-1.4 L29	N
Meteo-France	Spectral T63*L31	Bougeault (1985)	Moisture convergence	182GP*152GP L31	N
UKMO	Gridpoint 144*48*L19	Gregory and Rowntree (1990)	Cloud base buoyancy	1.25*0.3-1.25 L40	N

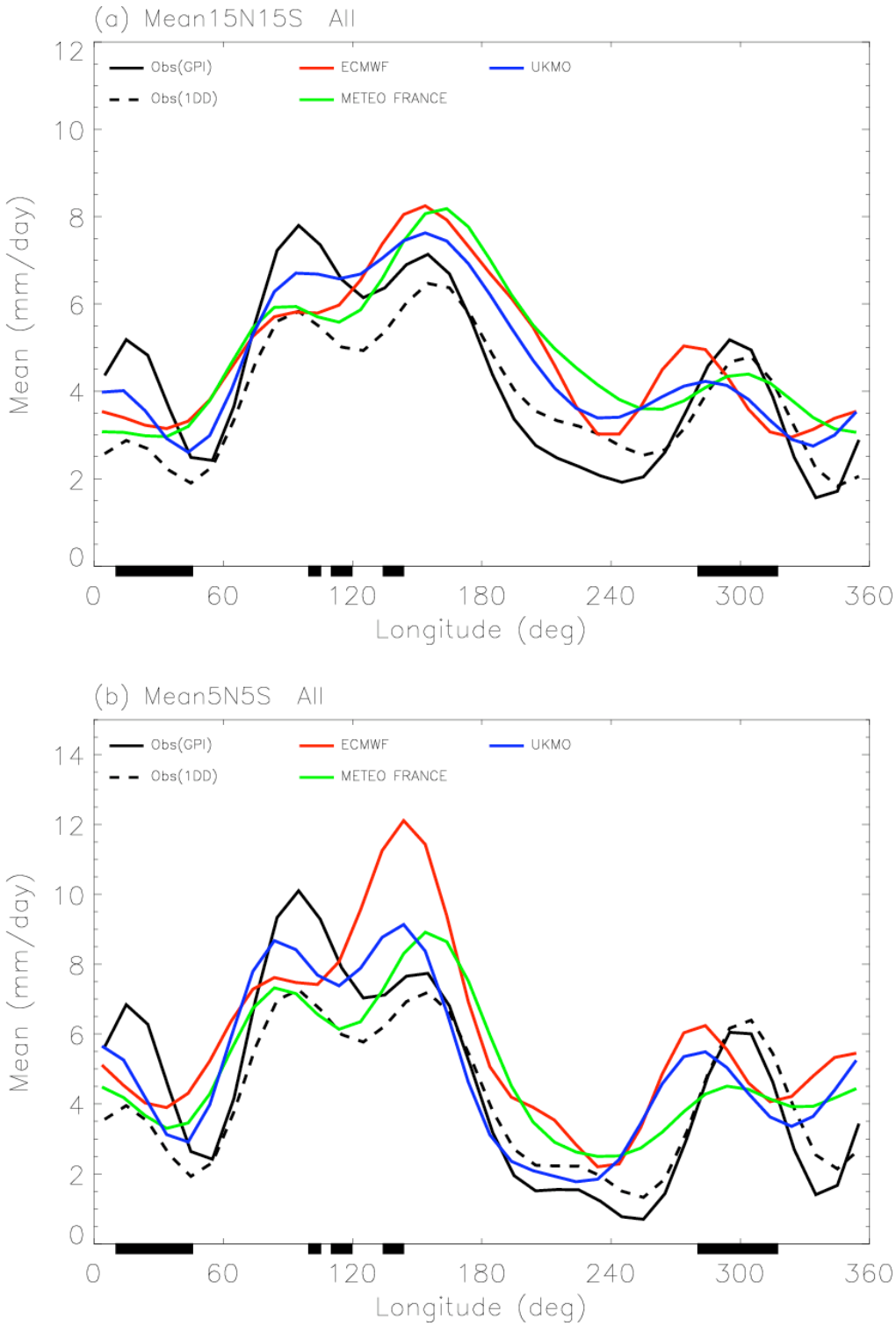

Figure 1. Annual mean precipitation along the equatorial belt averaged between (a) 15N and 15S, and (b) 5N and 5S for two observational datasets and 14 models. The data are smoothed zonally to keep only wavenumber 0-6. The locations of continents within the equatorial belt are indicated by black bars under the abscissa.

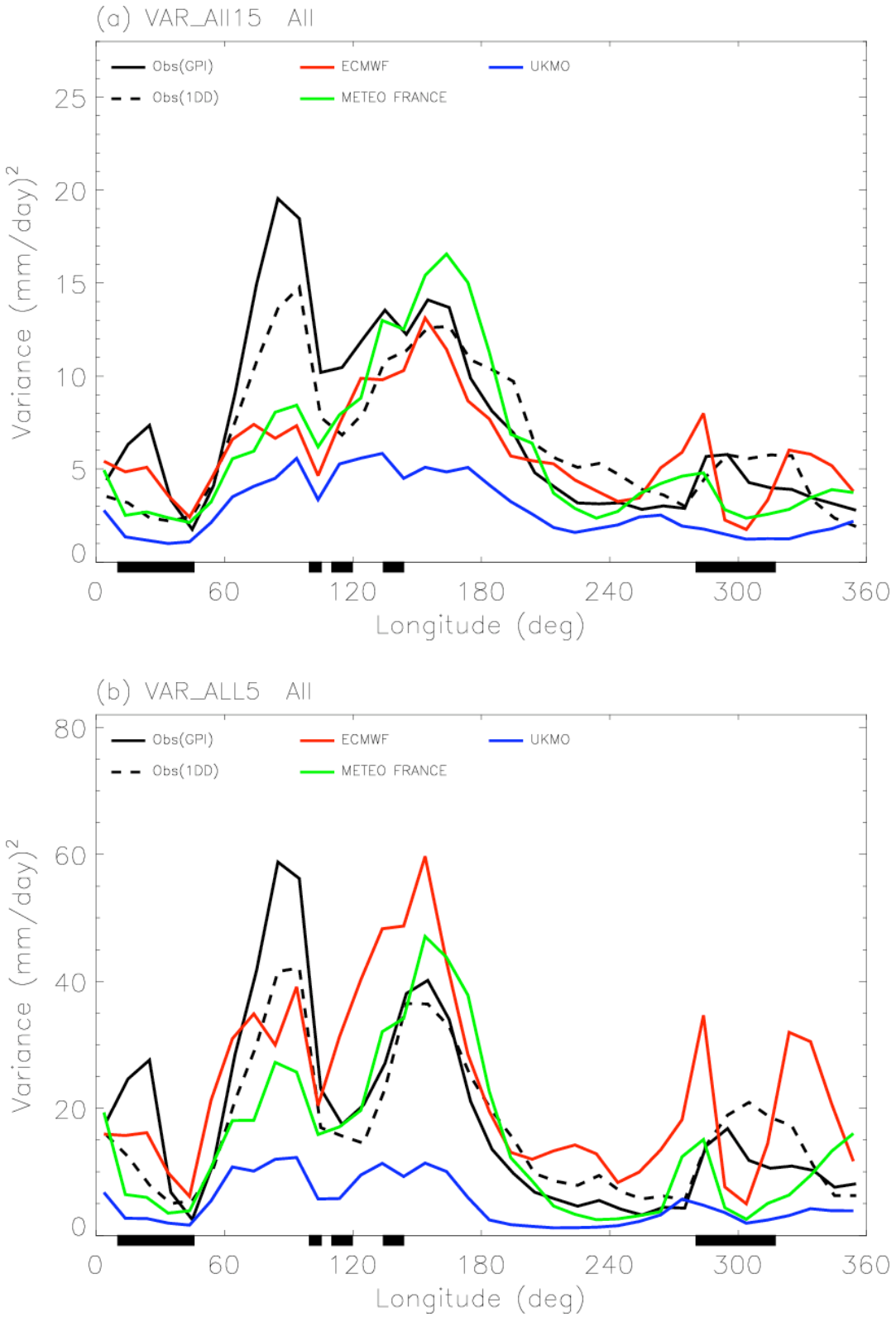

Figure 2. Variance of the 2-128 day precipitation anomaly along the equator averaged between (a) 15N-15S, and (b) 5N-5S.

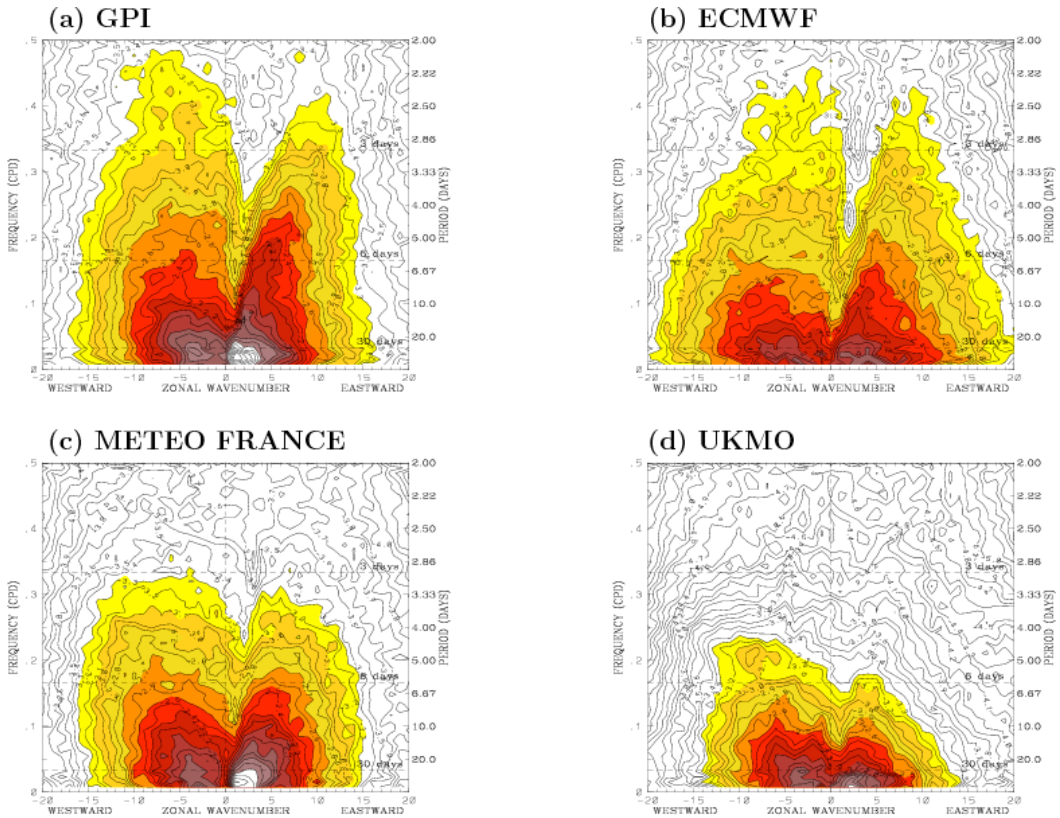

Figure 3. Space-time spectrum of 15N-15S symmetric component of precipitation. Frequency spectral width is 1/128 cpd.

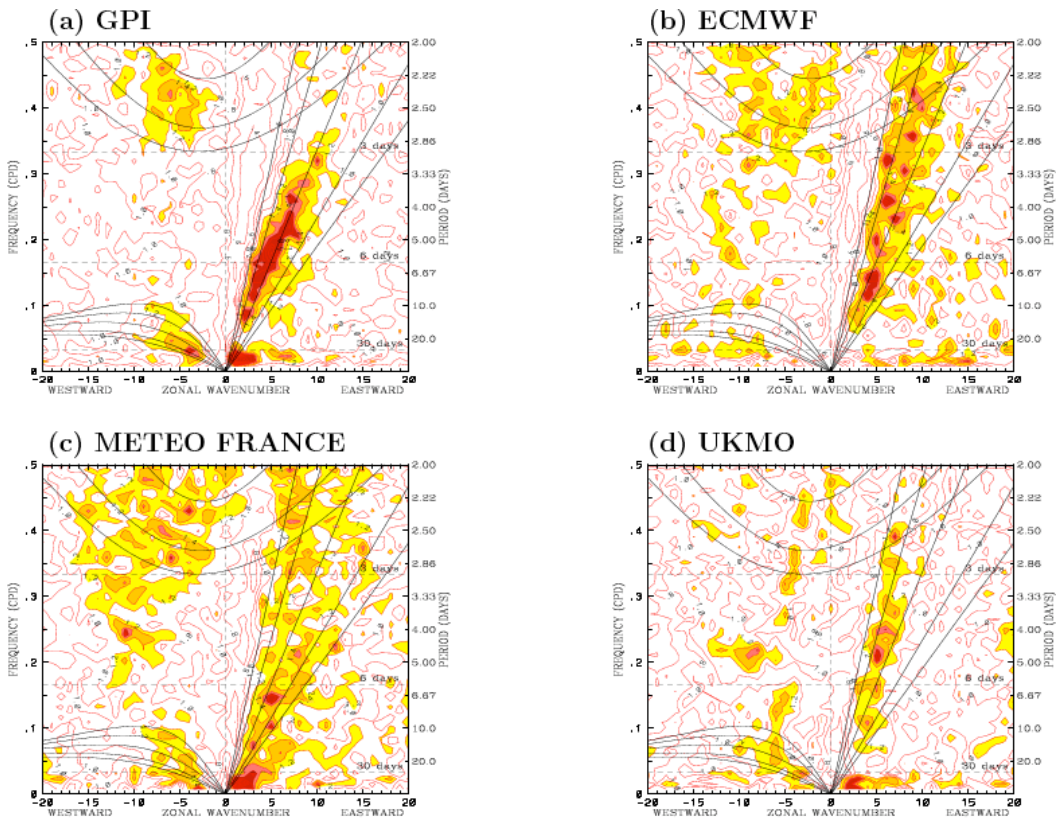

Figure 4. Space-time spectrum of 15N-15S symmetric component of precipitation divided by the background spectrum. Superimposed are the dispersion curves of the odd meridional mode-numbered equatorial waves for the five equivalent depths of 8, 12, 25, 50, and 90m. Frequency spectral width is 1/128 cpd.

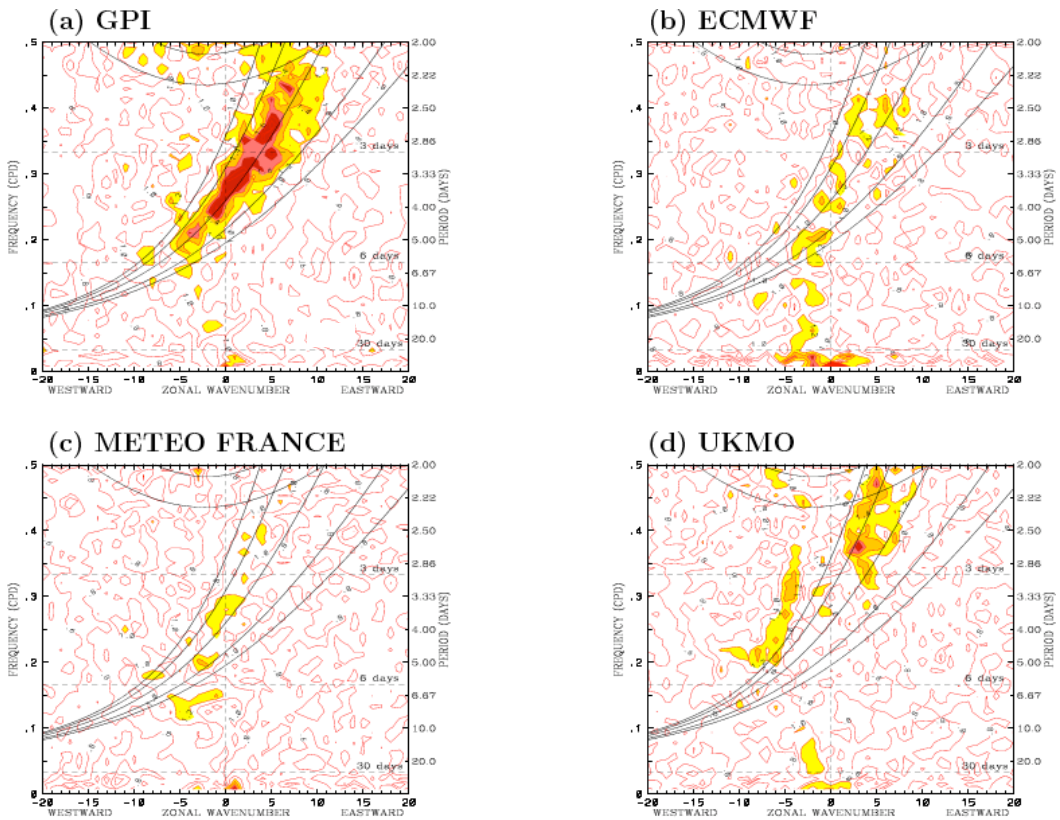

Figure 5. Same as Figure 4 but for the antisymmetric component.

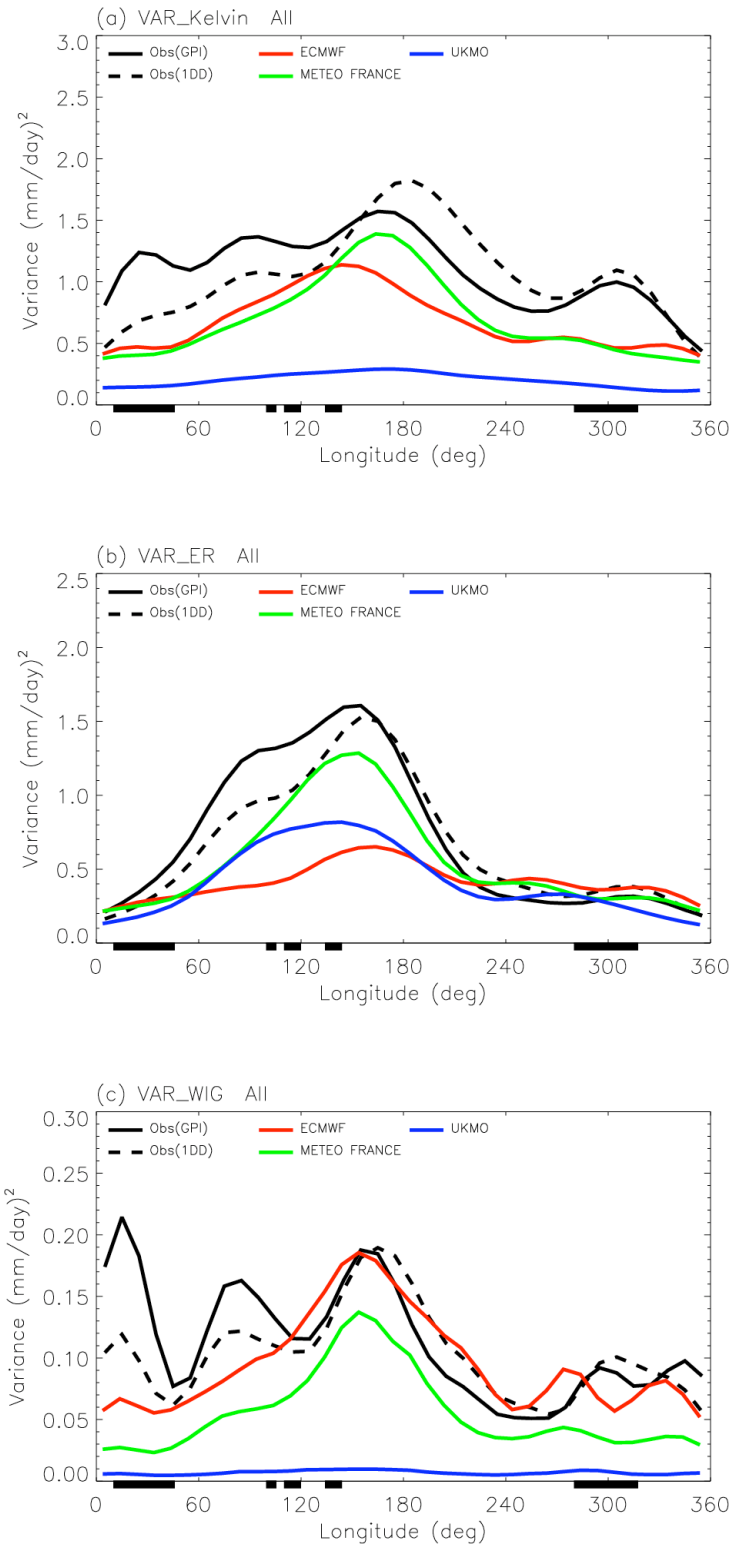

Figure 6. Variances of (a) Kelvin, (b) ER, and (c) WIG modes along the equator averaged between 15N and 15S.

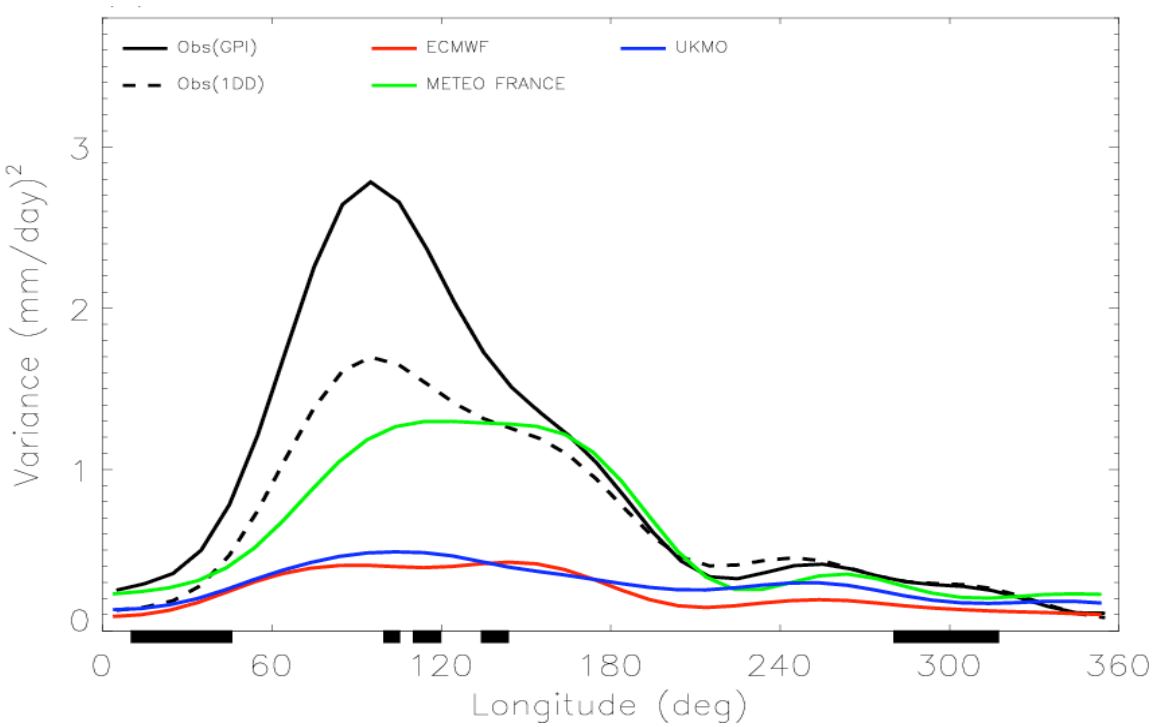

Figure 7. Variance of the MJO mode along the equator averaged between 15N and 15S.

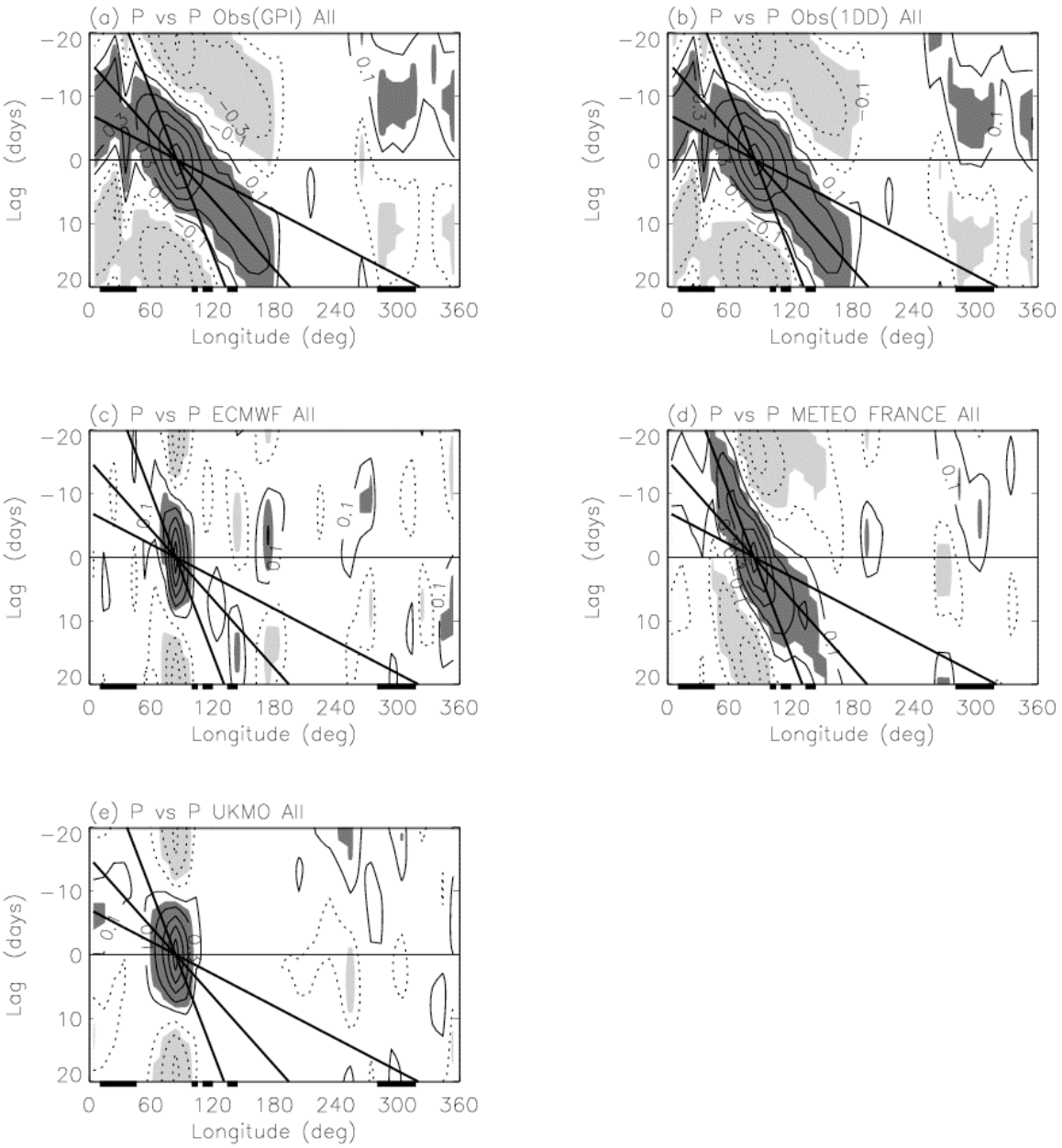

Figure 8. Lag-correlation of the 30-70 day precipitation anomaly averaged along the equator between 5N and 5S with respect to itself at 0N85E. Shading denotes the regions where lag-correlation is above the 95% confidence level. The three thick lines correspond to phase speed of 3, 7, and 15 m/s, respectively.

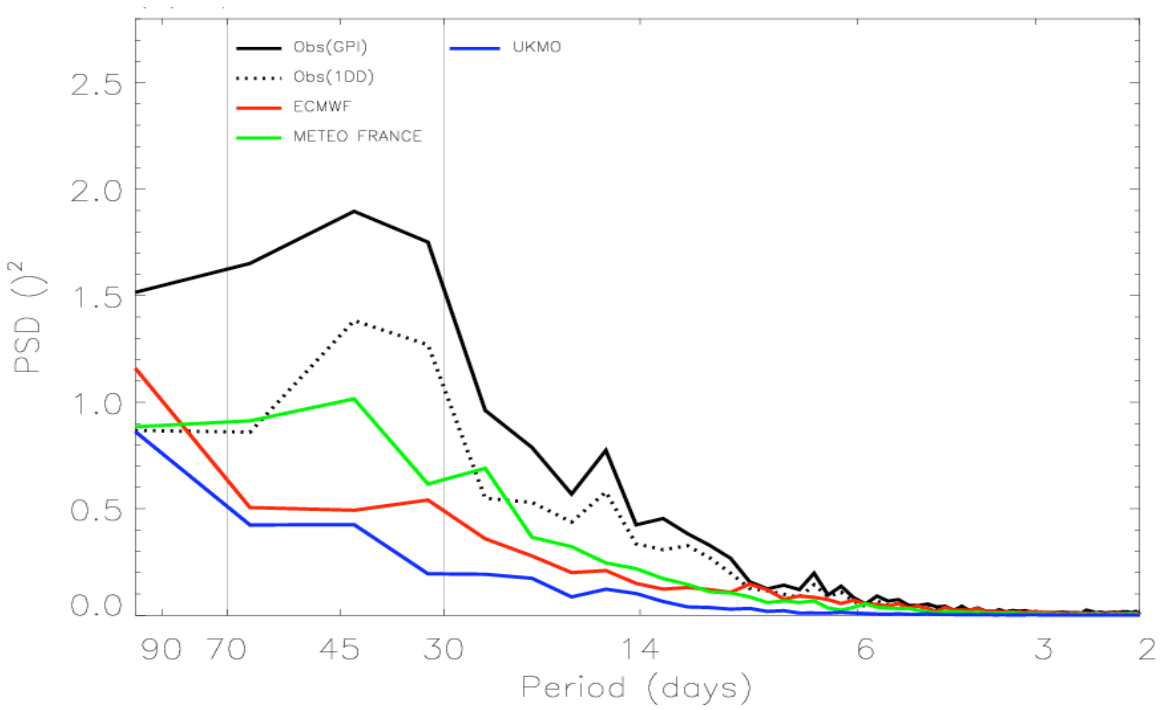

Figure 9. Spectrum of the eastward wavenumber 1-6 component of equatorial precipitation (5N-5S) at 0N85E for two observational datasets and 14 models. Upper panel: raw spectrum; Lower panel: normalized spectrum. Frequency spectral width 1/100 cpd.

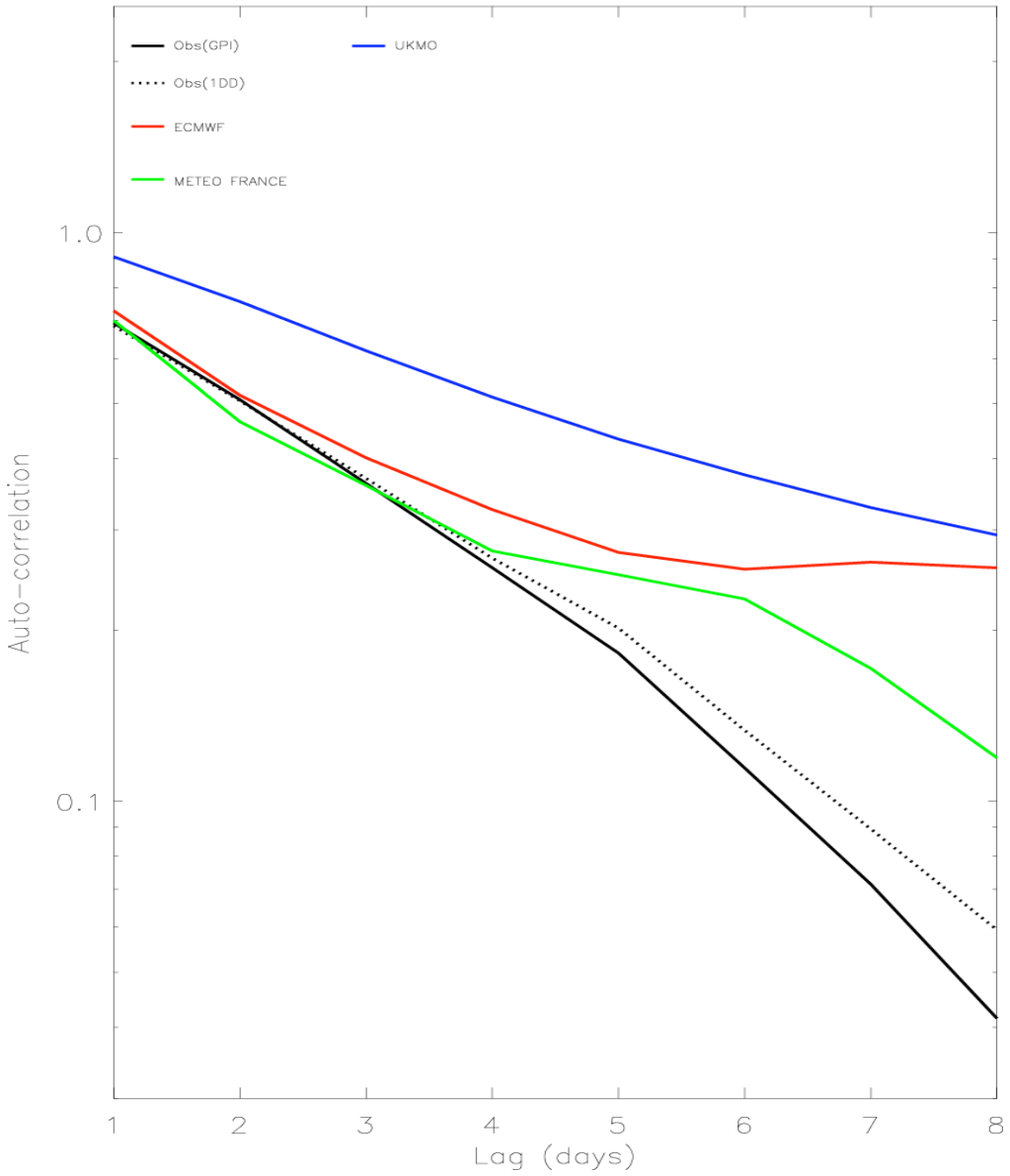

Figure 10. Auto-correlation of precipitation at 0N85E